Eur. Phys. J. D (2013)
DOI: 10.1140/epjd/e2013-40408-7

THE EUROPEAN PHYSICAL JOURNAL D

Regular Article

Hypergravity effects on glide arc plasma

Jiří Šperka[1,2,a], Pavel Souček[1], Jack J.W.A. Van Loon[3,4], Alan Dowson[4], Christian Schwarz[4], Jutta Krause[4], Gerrit Kroesen[5], and Vít Kudrle[1]

[1] Department of Physical Electronics, Masaryk University, Kotlářská 2, 61137 Brno, Czech Republic
[2] The Central European Institute of Technology (CEITEC), Masaryk University, Kotlářská 2, 61137 Brno, Czech Republic
[3] Dutch Experiment Support Center (DESC), ACTA-VU-University and University of Amsterdam, Amsterdam, The Netherlands
[4] European Space Agency (ESA), ESTEC, TEC-MMG, Noordwijk, The Netherlands
[5] Faculty of Applied Physics, Eindhoven University of Technology, P.O. Box 513, 5600 MB Eindhoven, The Netherlands

Received 11 July 2013 / Received in final form 18 October 2013
Published online (Inserted Later) – © EDP Sciences, Società Italiana di Fisica, Springer-Verlag 2013

Abstract. The behaviour of a special type of electric discharge – the gliding arc plasma – has been investigated in hypergravity ($1g$–$18g$) using the Large Diameter Centrifuge (LDC) at ESA/ESTEC. The discharge voltage and current together with the videosignal from a fast camera have been recorded during the experiment. The gliding of the arc is governed by hot gas buoyancy and by consequence, gravity. Increasing the centrifugal acceleration makes the glide arc movement substantially faster. Whereas at $1g$ the discharge was stationary, at $6g$ it glided with 7 Hz frequency and at $18g$ the gliding frequency was 11 Hz. We describe a simple model for the glide arc movement assuming low gas flow velocities, which is compared to our experimental results.

1 Introduction

The behaviour of electric discharges in altered gravity has, besides the aspect of fundamental research, also important practical consequences, like safety precautions in manned space flight and ion thrusters design [1,2].

It is known that some types of electric discharges are affected by gravity related processes. The electromagnetic forces between charged particles are typically much stronger than all gravitation forces acting and so the gravitation affects more the neutral particles (non ionised atoms and molecules). Generally, the electrostatic force is much stronger than the gravitational force, e.g. for electrons the ratio is about 10^{42}, for ions around 10^{34}. In reasonable external electric and gravity fields, the results are similar. In our experiment, the maximum electric field is around 10^6 V/m. The corresponding maximum acceleration of ion is in the order of 10^{14} m s^{-2}, i.e. still 13 orders of magnitude higher than $1g$ gravity acceleration.

These neutral particles are colliding with electrons and ions, transferring the momentum gained from gravity. Consequently, gravity affects the electrons and it can cause some changes in e.g. the electron energy distribution function. However, the research opportunities for this topic are rather limited, mainly due to the need of specialised equipment (deep mines, drop towers, centrifuges, parabolic flights, etc.) and thus there are still many open questions and problems.

[a] e-mail: georgejewel@gmail.com

In an electric discharge, the electrons are accelerated by the electric field and collide either elastically or inelastically with the gas molecules. The elastic collisions are generally much more frequent than the inelastic ones. Whereas the elastic collisons are responsible for a redistribution of kinetic energy, the inelastic collisions, namely the impact ionisation, are necessary for sustaining the discharge.

During the elastic collision, the transfer of energy between the electron and the atom or molecule is rather low due to the big inequality in their masses. In many types of laboratory plasmas, this leads to formation of a non-isothermal plasma, where the neutral gas has a much lower temperature than the electrons which are heated directly by the electric field. However, under certain conditions, sufficient frequency of electron-atom collisions can overcome this inefficiency and a nearly isothermal plasma is formed. A typical example is an electric arc, where the temperature of the neutral gas (and electrons, too) in the discharge column can reach several thousand Kelvin [3].

The difference in density of the heated gas in the discharge column and the cold surrounding atmosphere produces buoyancy which exerts a force on the plasma column. When the discharge is burning between two fixed points, it assumes a typical arc-like curved shape, which gave it the name – arc discharge. If the configuration of electrodes permits the movement of the plasma channel, a gliding arc is formed.

The sliding or gliding arc (glide arc) is a type of a plasma discharge, where the arc channel is moving along

slanted electrodes. The most probable place for arc ignition is the site of the strongest electric field, i.e. along the shortest path between the electrodes. Without buoyancy or external gas flow, the arc would stay in this place indefinitely. When external forces (buoyancy, gas flow) act on the plasma channel, it is pushed from this optimal position. However, the discharge has certain resistance or reluctance to be moved out of this optimal position due to the minimum energy principle (the power needed to sustain the discharge increases with discharge length [4]). The effect of arc gliding therefore needs that the external force overcomes the movement reluctance of the discharge, which is apparently dependent on the angle between the slanted electrodes. However, due to the microscopic surface irregularities affecting local electric field the situation is more complex and the force needed to move the discharge can be substantially higher. So for low gas flow and low buoyancy, the discharge will be stationary and situated near the shortest path between the electrodes and only for high gas flow and/or high buoyancy force it will act as a glide arc. The discharge also consecutively changes its properties from the ones nearly identical to a standard arc discharge at short channel lengths to a non-equilibrium plasma at longer channels. The non-equilibrium stage begins when the length of the plasma column exceeds its critical value and heat losses from the plasma begin to exceed the energy supplied by source. The maximum length of the glide arc channel is related to the supplied voltage. After the quenching of one discharge at maximum elongation a new discharge appears at minimal electrode distance and the whole evolution is repeated [4,5]. Typical discharge parameters are mentioned in [6]. Advantageous properties of the glide arc plasma can be used for various applications [7].

Besides buoyancy also other forces can influence the movement of the plasma channel. For example, a gas drag acts, when the discharge is operated in a flow regime. However, in our experiment we tried to minimize the gas flow to make the buoyancy force dominant.

Some types of laboratory plasmas have already been investigated in both hypergravity and microgravity conditions. One of the first to be investigated was the arc discharge in free fall [8,9]. Recently, several arc experiments have been carried out in both micro- and hypergravity. Carbon species were synthesized in microgravity [10] in the 28th ESA Parabolic Flight Campaign. Single-walled carbon nanotubes were produced by arc discharge method in hypergravity [11] and also microgravity [12,13]. The flow phenomena in metal-halide arc discharge lamps were intensively investigated under varying gravity conditions [14–16]. Low pressure radio frequency plasmas with dust particles are currently researched in various gravity conditions, too [17–19]. However, to our best knowledge, nobody has studied the gliding arc in hypergravity yet, despite its similarity to standard arc plasma.

In this paper we tried to advance and broaden previous research [11,12] and report on the first experimental results of a gliding arc under hypergravity conditions.

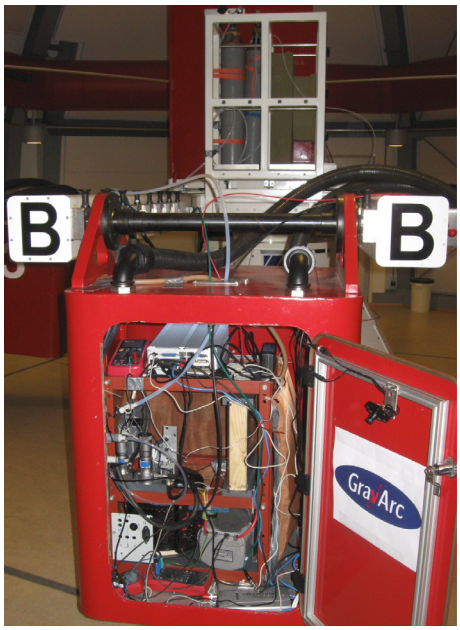

Fig. 1. The experimental setup installed inside the gondola. The gas bottles are situated in the center of the centrifuge.

2 Experimental section and methods

2.1 Description of the experimental apparatus

The experiments in hypergravity ($1g$–$18g$) were performed on the LDC which is part of the Life and Physical Sciences Instrumentation and Life Support Laboratory (LIS) at ESTEC (Noordwijk, the Netherlands) [20].

The weight bearing cage frame of the GRAVARC (GRAVity ARC) experimental setup is made of steel. As the whole experimental setup must fit into the LDC gondola (Fig. 1), the dimesions (length, width, height) were 46 cm, 38 cm and 58 cm, respectively. The weight of the complete experimental setup including the diagnostics was about 75 kg, so the construction of the device had to take into account the extreme forces at hypergravity. All heavy parts were properly fastened to the force-bearing frame of the experimental setup and the heaviest parts were placed on the bottom of the setup. The experiment was simply laid on the gondola floor and not hang-wired to its walls as there were no significant vibrations during the spin. The outer walls and some inner walls of the experimental setup were Faraday shielded by a conducting metal mesh.

The payload was divided into three sections. The lowermost power section contained a low voltage and a high voltage transformer. The middle section included the discharge chamber together with diagnostics. The uppermost section dedicated to control contained an industrial PC. Sensitive parts of the experiment, like grating spectrometer and gas bottles, were placed in the hub of the centrifuge. The schematic drawing of the whole experiment can be found on Figure 2.

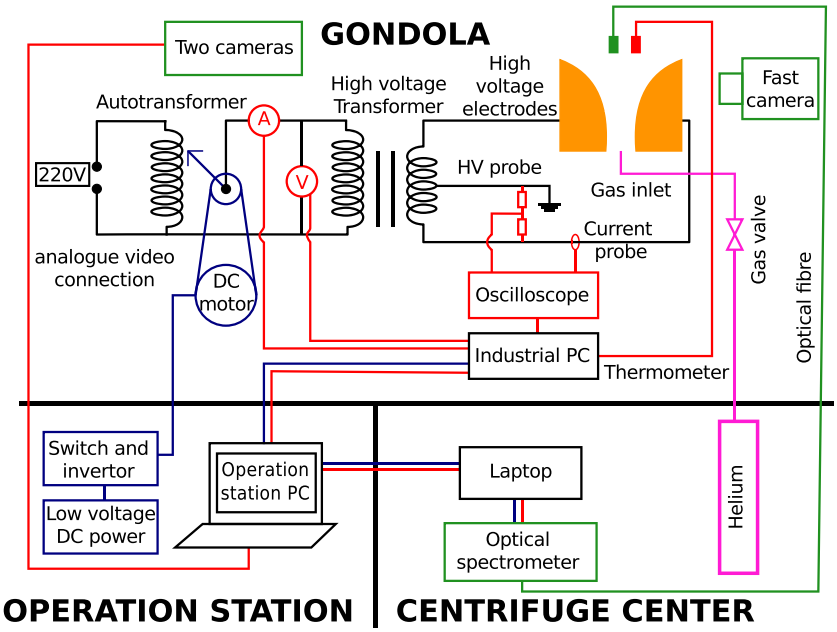

Fig. 2. Schematic drawing of the GRAVARC experiment. Discharge circuit and computers – black, diagnostics and data acquisition – red, control – blue, optical parts – green, gas supply – magenta.

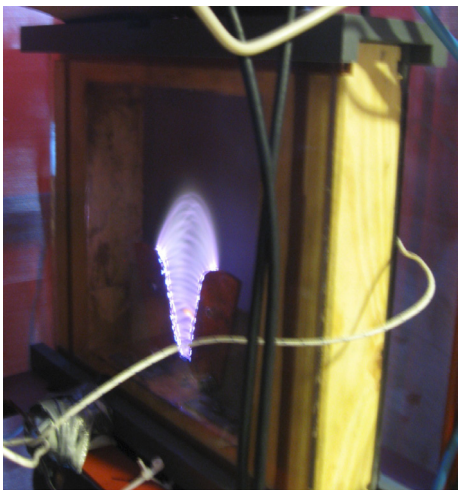

Fig. 3. The photograph of the installed discharge chamber with operating glide arc discharge under normal gravity conditions, exposure time 1 s. The helium gas flow $Q_{\mathrm{He}} = 40$ sccm, corresponding RMS voltage and current on the primary coil of the HV transfomer $U = 234$ V, $I = 5.5$ A.

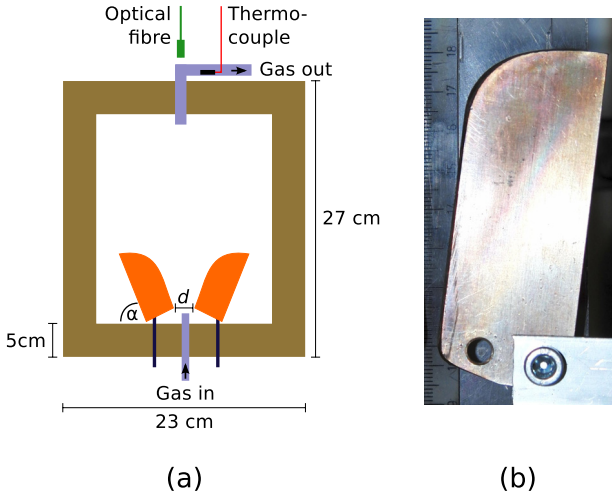

Fig. 4. (a) Schematic drawing of the discharge chamber, $d = 4.95$ mm and $\alpha = 72°$. (b) Photograph of one electrode. Ruler in cm included for scale.

2.2 Discharge chamber

The discharge chamber is visualised in Figures 3 and 4. The frame of the discharge chamber is made from spruce wood covered by mica, which protects the wood against direct contact with plasma. The outer dimensions of the chamber are 27 cm, 23 cm and 5 cm, the inner dimensions are 22 cm, 18 cm and 5 cm. The inner volume of the discharge chamber is 2 dm^3. The front and back walls of the discharge chamber are made from high temperature and thermal shock resistant glass. The back glass is sanded and blackened to avoid stray light reflections. A plastic sealing is compressed between the glass and the wood frame so the discharge chamber is reasonably air-tight with the exception of a venting hole at the top.

The electrodes have a shape close to a quarter ellipse. They are situated on the bottom of the discharge chamber and are made of 3.25 mm thick copper sheet. Their dimensions can be found on Figure 4b. Although the electrodes were movable, in the present study they stayed fixed (distance $d = 4.95$ mm and angle $\alpha = 72°$).

2.3 Electric and gas supply

The electric power was drawn from a standard power socket (230 V, 50 Hz) installed in the gondola via a fuse

and inrush current limiting thermistor. Using a remote controlled variable autotransformer we controlled the voltage on the primary winding of the high voltage (HV) transformer. The HV transformer, an inductance leakage type, has inherent current limitation. The maximum voltage on the secondary winding is 10 kV.

Helium gas continuously flows upwards through the discharge chamber. The gas is introduced and removed through fused silica tubes passing through the wooden frame. The gas flow was controlled using a calibrated needle valve. The effluent gas was released directly into the outer atmosphere.

2.4 Diagnostics

We employed several measurement techniques in order to study the glide arc discharge. All the data was continuously logged to the computer. We used an industrial computer with enhanced hypergravity resistance (sturdy design, fanless, solid-state disk storage, etc.). Where possible, opto-couplers on data lines were used to prevent electric hazard.

Two RS-232 equipped multimeters (type UNI-TREND UT70A, 3 readings/s) were used to measure the RMS (root mean square) voltage and current on the primary coil of the HV transfomer. A high voltage probe and a Rogowski coil were used to measure the discharge voltage and current. They were connected to a dual channel USB oscilloscope (Voltcraft DSO-2090).

Another RS-232 multimerer (type UNI-TREND UT70B, 3 readings/s) was used to monitor the temperature of the effluent gas using a K-type thermocouple. The thermocouple was placed directly inside the fused silica gas outlet – black square in Figure 4.

The high speed video of the discharge was recorded by a fast digital camera (Casio EX-ZR100) with a 224×160 resolution at frame rate 480 fps and saved on a secure digital (SD) memory card for later evaluation. Besides this one, two other cameras were placed in the gondola but only for monitoring purposes.

The fixed grating spectrometer Avantes Sensline AvaSpec-ULS-TEC (200–1100 nm, slit 25 μm, spectral resolution 0.34 nm) together with a controlling laptop was placed in the hub of the centrifuge to prevent adverse hypergravity effects on the fragile spectrometer. The 6 m long spectroscopic fibre (600 μm fused silica core diameter) gathered the plasma emission from the top, through the L-bent fused silica exhaust tube (Fig. 4). This configuration maximizes the light collected (as the discharge is always in the viewing angle of the fibre aperture) and it permits the recording of the UV spectra as the front glass is not transparent in the UV region.

2.5 Remote experiment control and monitoring

Throughout the experiments we remotely operated both computers, an industrial PC inside the gondola and standard laptop in the hub of the centrifuge from the control room (using Remote Desktop via ethernet connection). The data from the spectrometer, oscilloscope and digital multimeters was continuously acquired, logged and monitored directly during each experimental run. The data from the fast camera were stored on a high speed SD memory card during the run and transferred after spin-down. The camera limited the duration of a high speed video to 13 min.

In the control room, the output of the diagnostics instruments together with video feeds from two cameras were observed on the computer displays. One camera was focused on the discharge chamber to monitor the conditions of the discharge and the second camera overviewed the whole experimental set up.

The design of the experiment was very flexible – it can be operated with different electrode materials, various electrode spacing or angles and with various flows and composition of the working gas. However, the constraints of hypergravity engineering forced us to have only one remotely controlled parameter – the voltage on the HV transformer primary winding. The other parameters could be changed manually and only when the centrifuge was stopped. In this paper, all parameters except hypergravity and voltage were fixed.

The sliding brush of the variable autotransformer was moved by a geared DC motor. As the motor needed only low power, we were able to use cabling, originally (by centrifuge designers) intended for analog video signal. It connects the gondola and the control room via slip rings in the centrifuge hub. In the control room we used a simple reversing ON-OFF-ON switch to issue the commands UP, DOWN & STOP. This was done manually by the operator.

2.6 Experimental sequence

The experiments in hypergravity were generally done in the following sequence. Preparation phase: Helium gas flow was switched on for 10 min in advance to purge the discharge chamber, the connection between diagnostic instruments and control room was verified, the fast camera was started, the AC power of the variable autotransformer was switched on, the gondola was closed, all personnel left the LDC room. Second, the spinning phase, was observed from the control room, where three active operators managed the centrifuge, the remote control and the diagnostic outputs. Two backup operators observed the in-gondola video feeds, security limits (temperature, current, arcing, etc.) and made laboratory logs. The centrifuge was spin-up to the pre-set level, the electrode voltage was gradually increased until electric breakdown in helium. The centrifuge was programmed to follow a set of desired gravity levels, staying at one level for sufficient time to perform and log the data. At the end of the second phase the logging of the diagnostic data was stopped and the centrifuge was spun-down. In the third phase, the operators entered the LDC room, the gondola door was opened, the video from the SD card was transferred to data storage, the discharge chamber was let to cool down and helium gas flow was stopped.

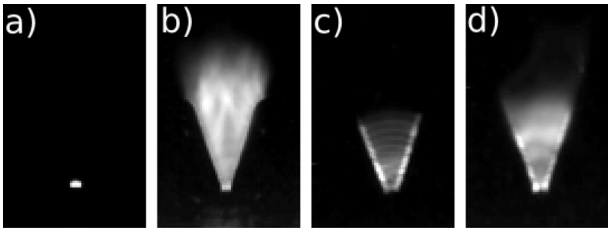

Fig. 5. Time-averaged images of approximately 700 fast camera frames for low (40 sccm) and high (170 sccm) helium flow: (a) $1g$, 40 sccm (b) $18g$, 40 sccm (c) $1g$, 170 sccm (d) $18g$, 170 sccm. The case of high flow and low gravity is visibly different from low flow and low gravity image due to the arc gliding in the former case and stable non-gliding arc in the latter case.

We made the experiments in the range of $1g-18g$. The centrifuge is able to reach $20g$, but only in the bottom part of the gondola. As our discharge chamber was situated near the center of the gondola, maximum hypergravity level was lower.

3 Results and discussion

All the experimentation worked flawlessly in hypergravity, including of-the-shelf components like multimeters, digital camera, etc. Only the oscilloscope exhibited some problems with relays responsible for range switching, which was solved by placing the oscilloscope on its back.

We tuned several experimental conditions (gas flow, inter-electrode distance and angle) to operate in buoyancy dominated regime and consequently near stationary arc – gliding arc transition. The increased buoyancy in hypergravity induced a transition from stationary arc (Fig. 5a) to gliding arc (Fig. 5b). The gravity level, at which the transition occurs, depends on experimental conditions (especially gas flow). In our experiment we observed this transition at $6g$. The experiments where the discharge was gliding even at $1g$ were performed, too (Fig. 5c). It was achieved by a higher gas flow. However, we were more interested in buoyancy dominated regime and by consequence, in low gas flow.

The graph in Figure 6 shows the temporal evolution of important macroscopic parameters – gravity, voltage and current on the primary side of the HV transformer and an effluent gas temperature – during one experimental run. The gas flow was constant, $Q_{\mathrm{He}} = 40$ sccm (standard cubic centimeters per minute). We can observe that the centrifuge was spun up to 12 g and only then the attempts to breakdown were started. It was achieved around $t = 13$ s. As the sustaining voltage is generally lower than the breakdown voltage, we tried to decrease the voltage a little. However, the discharge extinguished ($t = 20$ s) and so we increased the voltage again until a new breakdown. We tried to compensate again and after $t = 45$ s the glide arc was stable and so the voltage $U = 234$ V (RMS value) was left constant for the rest of the experiment. The corresponding RMS current in the primary winding

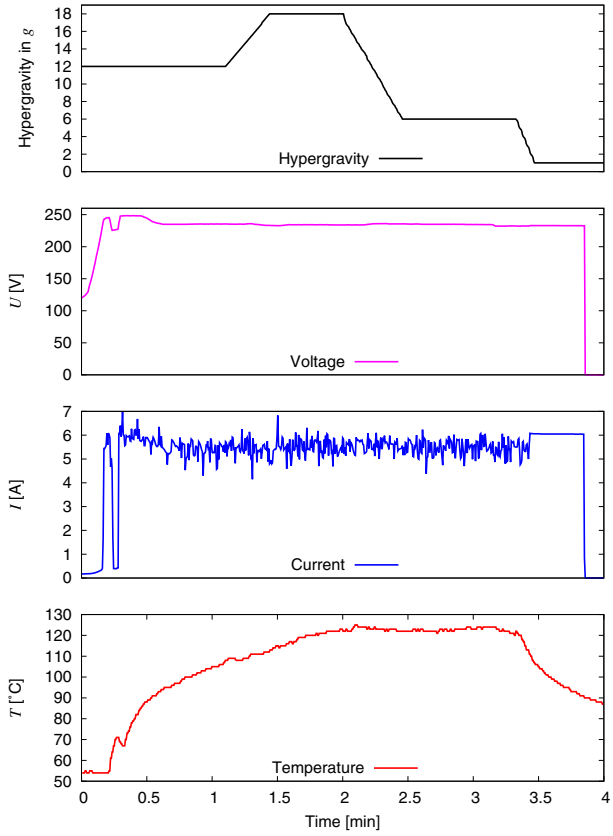

Fig. 6. Hypergravity levels, primary voltage U, primary current I and effluent gas temperature T plotted over the same time scale. The voltage $U = 234$ V is stable except an initial phase of an adjustment of the voltage (ca 30 s).

was oscillating around a mean of $I = 5.5$ A. It apparently does not depend on gravity. Our experiment started with discharge chamber preheated to 55 °C by the previous experiments. At time $t = 13$ s the plasma ignition was achieved. Since then, the temperature of the effluent gas gradually increased as the gas inside the discharge chamber got heated by the plasma. Concurrently, the resident gas was cooled down by the incoming gas and by discharge chamber walls. After certain time a dynamic equilibrium was achieved and the effluent temperature stabilised at 122 °C. Generally, the glide arc heat output could vary with the gravity due to changed convective heat transfer [21]. After spin-down to $1g$ (reached at 3 min 30 s) the discharge transformed from the gliding arc to a stationary arc discharge burning between the nearest parts of the electrodes due to the reduction of the buoyancy force. This proved that the parameters of our experiment were set correctly, i.e. the dominant force for channel movement was buoyancy, not gas flow. The effluent gas temperature began to decrease immediately (Fig. 6). This is caused by less efficient heating of the gas in chamber by the stationary arc with short discharge channel length. The effluent gas temperature strongly depends on the mode of the discharge (stationary/gliding).

The response of the discharge on altered gravity conditions was virtually instantaneous, so that the diagnostics

Table 1. Discharge parameters obtained from fast videos: f_g – characteristic frequency of plasma channel gliding, Δt – discharge channel lifetime, v_g – plasma channel movement speed and the distance l_{max} the channel travels in vertical direction between its ignition and disappearance.

gravity level	f_g [Hz]	Δt [ms]	v_g [cm s^{-1}]	l_{max} [mm]
$1g$	0	∞	0	0
$6g$	7	150	30	44
$12g$	9	110	38	42
$18g$	11	90	46	41

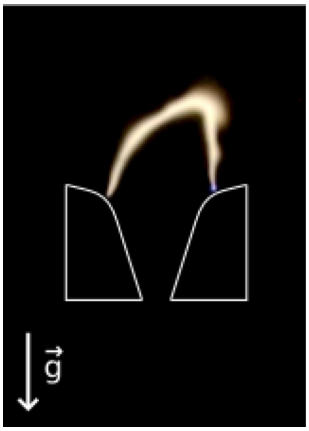

Fig. 7. Typical image of the glide arc at maximum expansion (just before extinguishing) at $6g$ as taken by the fast camera (480 fps, exposure time 2.1 ms).

experiments were done fairly quickly. The described diagnostic run took about 5 min, hypergravity was changed in steps (sequence $12g$, $18g$, $6g$, $1g$), requiring only a short time at each hypergravity level (100 s at $12g$, 40 s at $18g$ and 40 s at $6g$). When changing gravity level, the centrifuge was able to accelerate or decelerate very quickly, in around 30 s.

We visually observed that the speed of the plasma channel moving along the electrodes increases with gravity. This is caused by increased buoyancy at higher gravities. The same effect was observed in high speed camera recordings. From frame-to-frame image analysis we calculated the characteristic frequency of plasma channel gliding, discharge channel lifetime, plasma channel movement speed and the distance l the channel travels between its ignition and disappearance (see Tab. 1). The rates of new ignition are strongly dependent on gas flow rate [22]. It arises from our experiment that this phenomena depends also on gravity.

Figure 7 shows an typical characteristic shape of the glide arc plasma channel (taken from high speed 480 fps video) at its highest expansion just before its disappearance. This is already the non-equilibrium phase of the glide arc discharge development which is in its final phase. The discharge channel has reached its maximum length. It is apparent that the light emission differs in various areas of the discharge: bright electrode spots (contact points between the arc channel and the electrodes) are bluish but

Table 2. Discharge channel length obtained from fast videos.

time [ms]	$1g$ [mm]	$6g$ [mm]	$12g$ [mm]	$18g$ [mm]
0	3.15	3.2	4.1	4.1
20	3.15	4.5	6.8	5.9
40	3.15	8.1	12.2	11.7
60	3.15	11.7	19.4	18.5
80	3.15	14.9	30.2	30.6
100	3.15	18.9	45.0	–
120	3.15	26.6	–	–
140	3.15	39.6	–	–

the central part of the discharge is diffusive and yellowish. The visual appearance also suggests that there is present small amount of the outer atmosphere inside the discharge chamber.

During our experiment the discharge burning in $1g$ was a standard arc without any gliding. In higher gravities the buoyancy forced the discharge into the glide arc regime. Figure 8 shows time resolved evolution of the glide arc in different gravity conditions. In $6g$ the arc is quite round, in $12g$ and $18g$ the channel exhibits higher kurtosis. Increasing gravity, the buoyant force and therefore also the speed of movement increases. This makes the gas flow more dynamic and turbulent. This is evidenced by increasingly complex shapes of the plasma channel. The processes of gas flow, heat flow and electric current flow in turbulent medium are mutually interlinked, which makes theoretical treatment rather difficult and out of scope of this paper. In Table 2 there are discharge channel lengths for different time development which has been estimated from the image series. The plasma column length gradually increases during one glide arc period, while the arc length for the arc regime at $1g$ remains constant. The thickness of the discharge channel also evolves during one gliding period. The channel thickness is about 2 mm after the ignition for shortest channel length and increases up to 6 mm for largest discharge channel length. On the top of first pictures of all series from different g levels one may observe the afterglow of the previous plasma column, as it is decaying in the same time as the ignition of a new plasma column takes place.

We analysed the vertical position of the discharge on time using Figure 8. As a reference spot we chose the centre of the discharge channel between the electrodes. The results are shown in Figure 9. The velocity of the discharge channel for a given g is nearly constant. The discharge channel velocities determined from linear fit are 30 cm s^{-1} for $6g$ (3% uncertainty), 38 cm s^{-1} for $12g$ (3% uncertainty) and 46 cm s^{-1} for $18g$ (5% uncertainty), (see Tab. 1). The velocities clearly depend on g level, so the movement of the plasma channel was not caused by helium gas inflow. Taking into account the 40 sccm flow and 3 mm diameter of the inlet, we arrive at gas velocity of 9.5 cm s^{-1} directly in the inlet cross-section. In the discharge area, the induced flow is even lower due to bigger distance from the gas inlet. We estimate the gas velocity in the discharge area around 1 cm s^{-1}. This is quite negligible in comparison with observed arc channel velocities.

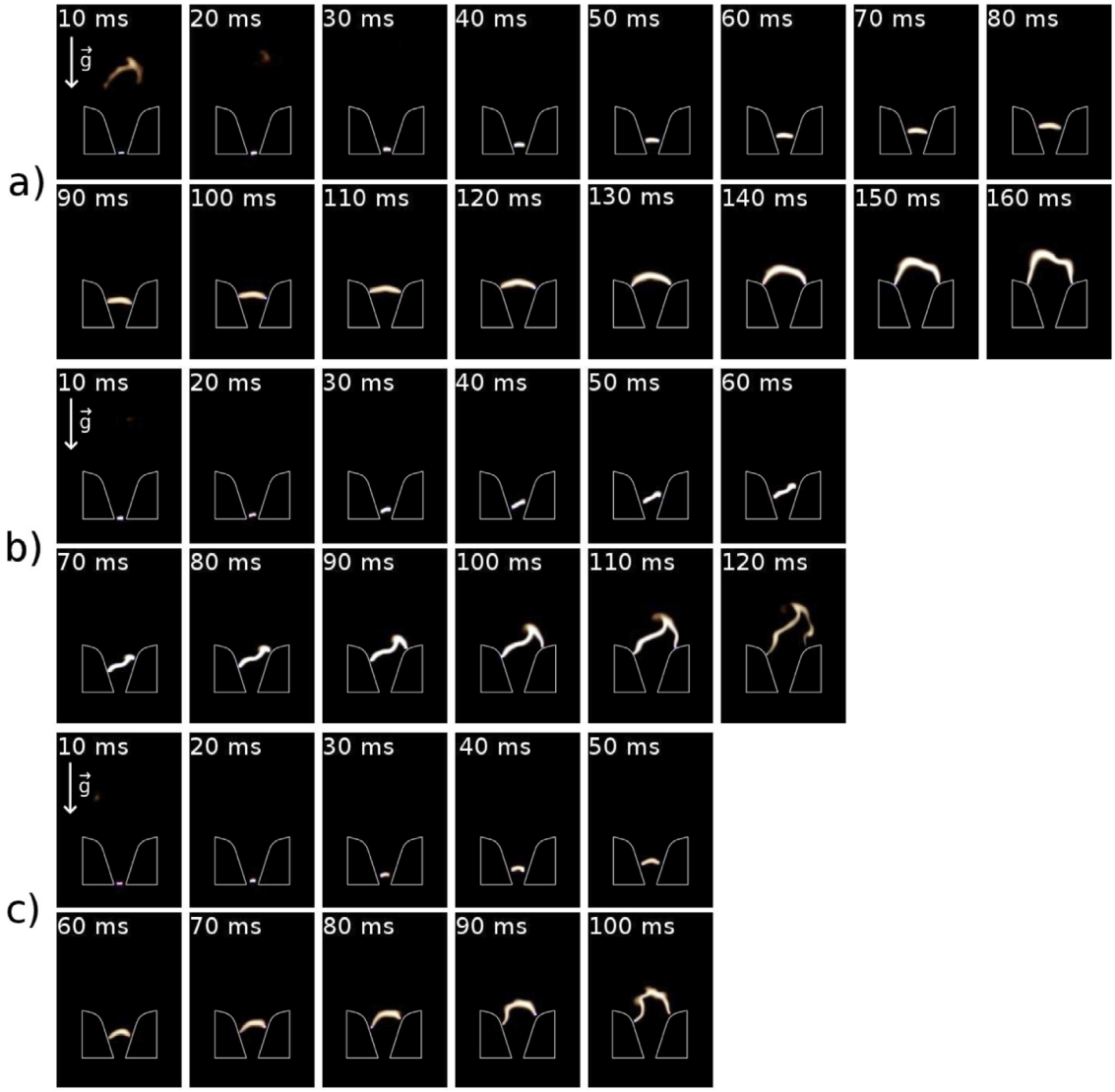

Fig. 8. Images of one glide arc glide at (a) $6g$ (b) $12g$ (c) $18g$ as taken by the fast camera. The time delay between two pictures is 0.01 s.

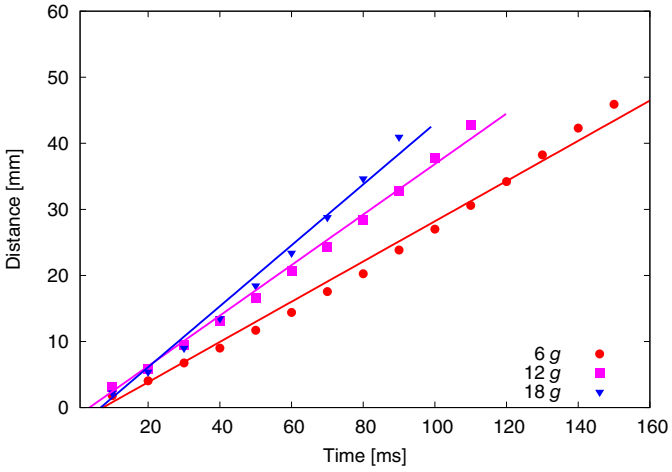

Fig. 9. Linear fits to the distance crossed by the glide arc at $6g$, $12g$ and $18g$.

Moreover, at $1g$ the arc did not move at all. The plasma column velocity was investigated by [23] in gliding arc with similar geometry, but for much higher gas flows (6–27 slm). In their case the plasma movement (900 cm s^{-1}) was caused by this strong gas flow and not by the buoyancy, so the results are not directly comparable with ours.

Due to the constraints of LDC scheduling, we did not repeat the whole experimental run (i.e. series with preprogrammed gravity levels and discharge voltages). However, each data point in Tables 1 and 2 and Figure 9 is in fact an average from behaviour of many individual filaments. The relative statistical error was below 20%. The gliding of the filaments is inherently stochastic phenomena and so some spread of the values is to be expected. The statistics of the filament motion can be observed on time integrated images in Figure 5. These are normalized sums of approx. 700 frames from fast camera, which is practically equivalent to long exposure (∼0.5 s) standard photography.

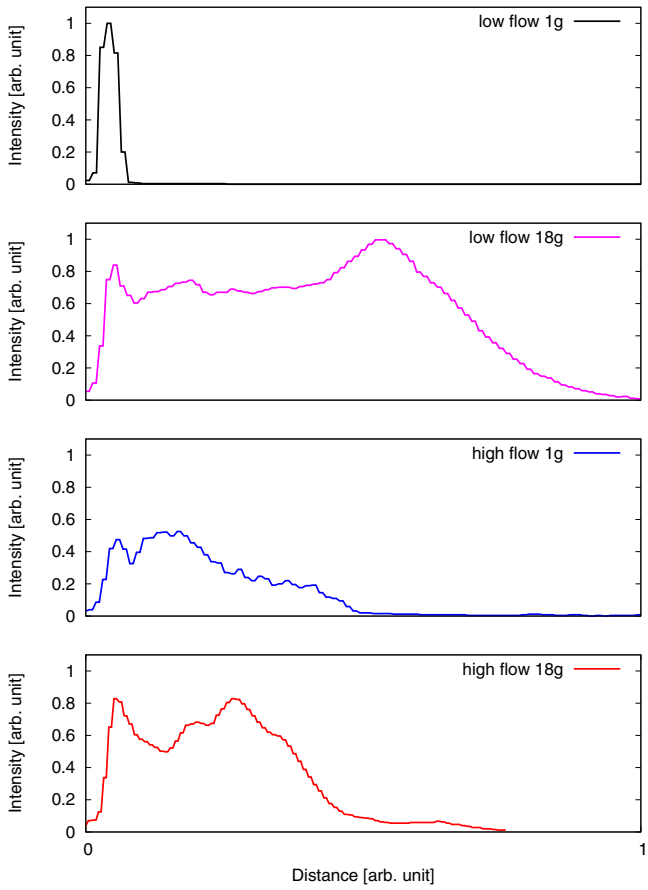

Fig. 10. Intensity profiles along vertical axis of four images from Figure 5. The tail of the profile reflects the statistics of stochastic filament movement.

Although the bottom part of the interelectrode area is saturated, in the top part the gradual decrease of the intensity is directly proportional to cumulative distribution of maximum heights reached by the individual filaments. When intensity profile of such images along the vertical axis is plotted (see Fig. 10), the distribution is even more clear. The probability of finding the filament in certain position can be deduced from the corresponding tail of the intensity profile.

We tried to estimate the terminal velocity of the arc channel when gravity, buoyancy and aerodynamic drag are considered. Let us suppose that the rising plasma column can be approximated by a cylinder of hot gas with its axis normal to its movement in surrounding cold gas. This is reasonable approximation in the case of the glide arc [24,25]. The drag equation is in the form

$$F_{\mathrm{D}} = \frac{1}{2}\,\rho_2 v^2 C_{\mathrm{D}} A, \tag{1}$$

where F_{D} is the drag force, ρ_2 is the density of the surrounding gas, v is the speed of the object relative to the fluid, A is the cross-sectional area and C_{D} is the drag coefficient. Using this equation and assuming simple Archimedes upward buoyant force acting on the cylinder we can estimate the equilibrium (terminal) velocity of the

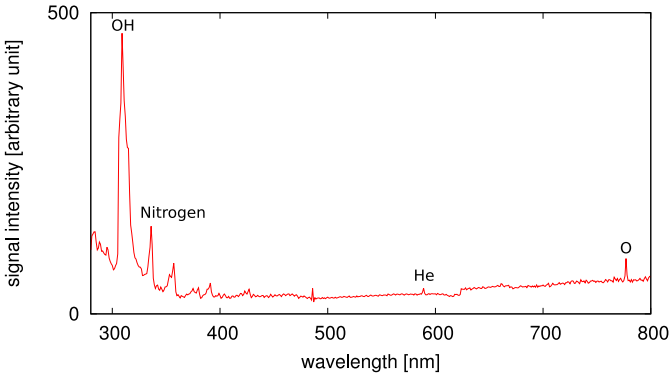

Fig. 11. Optical emission spectrum of the discharge at $12g$. OH at 309 nm, N_2 at 316 nm, 336 nm and 357 nm, atomic oxygen line at 777 nm and weak peak of helium at 587 nm.

cylinder in a following form

$$v = \sqrt{\frac{\pi r g(1-\frac{\rho_1}{\rho_2})}{C_{\mathrm{D}}}} = \mathrm{const}\sqrt{g} \tag{2}$$

where r is the cylinder radius, ρ_1 is the density of the hot gas inside the cylinder and g is gravity. The densities ρ_1 and ρ_2 naturally depend on gas and filament temperatures, which in turn could depend on the gravity level. The temperature of the surrounding gas inside the discharge chamber slightly changed during the experiment. However, during the experimental part, which was considered for later evaluation (from 45 s), the effluent gas temperature difference was no more than 45 °C (Fig. 6). Also the temperature of the plasma filament itself does not significantly change with varying gravity. This is supported by the results of the OES. So in effect the square root of $(1-\frac{\rho_1}{\rho_2})$ in equation (2) does not significantly change with gravity and the gliding velocity should depend on the square root of gravity level.

The approximate average radius of the discharge channel is in our case $r = 2$ mm, the density of helium at room temperature at atmospheric pressure $\rho_2 = 0.18$ kg m^{-3}, the density of helium at 3000 K at atmospheric pressure $\rho_1 = 0.016$ kg m^{-3} and we can consider the drag coefficient C_{D} equal to 1.8 which corresponds to the Reynolds number equal to 80 [26], which approximately corresponds to our experimental conditions. Substituting this values into equation (2) one gets velocities 15.2 cm s^{-1}, 21.5 cm s^{-1} and 26.3 cm s^{-1} corresponding to $6g$, $12g$ and $18g$. These velocities, despite being calculated from very simple model, are similar to the measured values. The biggest deficiencies of the model are the consideration of the solid object and the estimation of drag coefficient which strongly depends on shape and on the Reynolds number. Moreover, both the experiment and model exhibit the square root dependency of v on g level.

The strong bands of N_2 and OH in a typical optical emission spectrum (Fig. 11) indicates a presence of air in the discharge chamber. Although the helium line is weak in comparison to these impurities, it can not be directly interpreted as a strong contamination of the discharge

volume. It is well known that impurities are very strong in emission even in mixtures where their abundance is very low. E.g. authors [27] observed strong N_2 bands in very pure (better than 10 ppm) helium atmosphere. This effect is caused by very high first excitation level of He, which for typical electron energy (less than several eV) makes the impurities much more easily excited than He atoms. We did not observe any significant changes in emission spectra, especially in the shape of OH band, which could be attributed to change of plasma channel temperature with gravity. This validates the simplified treatment in equation (2). The spectroscopically proven presence of impurities, i.e. the gas of different mass density, should lead to a gravity induced separation of the gases [14]. Unfortunately, in our experimental set-up we can not observe that because we measure the spectra from above, i.e. in a vertically averaged way. Similarly, the dynamic effects of gliding arc in varying gravity are also not observable due to vertical integration and rather long exposure times. Therefore we must conclude that at the level of confidence limited by low spectral resolution and virtually non-existent temporal and spatial resolution, the gravity level has not any significant effect on the plasma emissions.

4 Conclusions

A new experimental device has been constructed to perform measurements on an atmospheric pressure glide arc helium plasma under hypergravity conditions up to $18g$ using the LDC at ESTEC.

Gravity strongly influenced the glide arc discharge. We explain these effects by thermal buoyancy, which increases with gravity. The experimental conditions were set so close to the arc – glide arc transition, that the change of regimes appeared only by increasing gravity. The arc plasma did not move under normal gravity conditions. In the gliding arc regime, increasing gravity led to a higher gliding speed of the plasma channel (30 cm s^{-1} at $6g$, 38 cm s^{-1} at $12g$ and 46 cm s^{-1} at $18g$) and higher frequency of appearance/disappearance (7 Hz at $6g$, 9 Hz at $12g$ and 11 Hz at $18g$). The velocity of the plasma column was constant during one glide arc cycle. Presented simple analytical model of the glide arc plasma column predicts that its velocity depends on $\sqrt{g}$. This is in good agreement with our experimental results.

This work was supported by the European Space Agency, by Masaryk University, by Central European Institute of Technology (CZ.1.05/1.1.00/02.0068) funded by European Regional Development Fund, by the Czech Science Foundation (104/09/H080) and by project CZ.1.05/2.1.00/03.0086 funded by European Regional Development Fund. We wish to acknowledge the help provided by Czech Space Office, AVANTES and FEI company. A special thank goes to ESA Education office for the great Spin Your Thesis! 2012 programme. We are particularly grateful for the assistance given by Natacha Callens and Tim Setterfield. We would like to thank also our skilled technicians Petr Saul, Tomáš Saul and Pavol Bzinčák for helping us with the construction of the GRAVARC experiment.

References

1. K.G. Balmain, J. Electrost. **20**, 95 (1987)
2. H. Huang, W. Pan, C. Wu, IEEE Trans. Plasma Sci. **39**, 2934 (2011)
3. M. Baeva, R. Kozakov, S. Gorchakov, D. Uhrlandt, Plasma Sources Sci. Technol. **21**, 055027 (2012)
4. A. Fridman, S. Nester, L.A. Kennedy, A. Saveliev, O. Mutaf-Yardimci, Prog. Energy Comb. Sci. **25**, 211 (1998)
5. X. Tu, L. Yu, J.H. Yan, K.F. Cen, B.G. Chéron, Phys. Plasmas **16**, 113506 (2009)
6. A. Czernichowski, Pure Appl. Chem. **66**, 1301 (1994)
7. J. Janča, A. Czernichowski, Surf. Coat. Technol. **98**, 1112 (1998)
8. M. Steenbeck, Z. Tech. Phys. **18**, 593 (1937)
9. C. Kenty, J. Appl. Phys. **10**, 714 (1939)
10. V. Pletser, Acta Astronaut. **55**, 829 (2004)
11. G.D. Tan, T. Mieno, Thin Solid Films **518**, 3541 (2010)
12. O. Kawanami, N. Sano, T. Miyamoto, A. Mineshige, T. Murakami, H. Harima, Appl. Phys. A **89**, 929 (2007)
13. J.M. Alford, G.R. Mason, D.A. Feikema, Rev. Sci. Instrum. **77**, 074101 (2006)
14. W.W. Stoffels, A.J. Flikweert, T. Nimalasuriya, J. Van der Mullen, G.M.W. Kroesen, M. Haverlag, Pure Appl. Chem. **78**, 1239 (2006)
15. A.J. Flikweert, T. Nimalasuriya, G.M.W. Kroesen, M. Haverlag, W.W. Stoffels, Microgravity Sci. Technol. **21**, 319 (2009)
16. T. Nimalasuriya, A.J. Flikweert, M. Haverlag, P.C.M. Kemps, G.M.W. Kroesen, W.W. Stoffels, J. Van der Mullen, J. Phys. D **39**, 2993 (2006)
17. C.R. Du et al., New J. Phys. **14**, 073058 (2012)
18. K. Takahashi, Y. Hayashi, S. Adachi, J. Appl. Phys. **110**, 013307 (2011)
19. J. Beckers, T. Ockenga, M. Wolter, W.W. Stoffels, J. van Dijk, H. Kersten, G.M.W. Kroesen, Phys. Rev. Lett. **106**, 115002 (2011)
20. J.J.W.A. van Loon, J. Krause, H. Cunha, J. Goncalves, H. Almeida, P. Schiller, *Proc. Of the Life in Space for Life on Earth Symposium, Angers, France, 2008*, ESA SP-663
21. D.B. Ingham, I. Pop, *Convective heat transfer: mathematical and computational modelling of viscous fluids and porous media* (Access Online via Elsevier, Elsevier, 2001)
22. Z.W. Sun, J.J. Zhu, Z.S. Li, M. Aldén, F. Leipold, M. Salewski, Y. Kusano, Opt. Express **21**, 6028 (2013)
23. Z. Bo, J.H. Yan, X.D. Li, Y. Chi, B. Chéron, K.F. Cen, Plasma Chem. Plasma Process. **27**, 691 (2007)
24. S. Pellerin, F. Richard, J. Chapelle, J.M. Cormier, K. Musio, J. Phys. D **33**, 2407 (2000)
25. F. Richard, J.M. Cormier, S. Pellerin, J. Chapelle, J. Appl. Phys. **79**, 2245 (1996)
26. R.K. Finn, J. Appl. Phys. **24**, 771 (1953)
27. M. Bogaczyk, R. Wild, L. Stollenwerk, H.E. Wagner, J. Phys. D **45**, 465202 (2012)